Interactions of the α-subunits of heterotrimeric G-proteins with GPCRs, effectors and RGS proteins: A critical review and analysis of interacting surfaces, conformational shifts, structural diversity and electrostatic potentials

Fotis A. Baltoumas[a], Margarita C. Theodoropoulou[a], Stavros J. Hamodrakas[a]*

Fotis A. Baltoumas: fotis.baltoumas@gmail.com; Margarita C. Theodoropoulou: mtheodo@biol.uoa.gr; Stavros J. Hamodrakas: shamodr@biol.uoa.gr

[a] Department of Cell Biology and Biophysics, Faculty of Biology, University of Athens, Panepistimiopolis, Athens 157 01, Greece

* Corresponding Author. Address: Department of Cell Biology and Biophysics, Faculty of Biology, University of Athens, Panepistimiopolis, Athens 157 01, Greece. Phone: +30-210-7274931, Fax: +30-210-7274254, e.mail: shamodr@biol.uoa.gr

Supplementary Material

Figure S1. Multiple sequence alignment of the RGS domains of RGS proteins with known structure. **A**. Representation of sequence similarities using the Clustal X color code. **B**. Representation of Gα interacting residues, as indicated by crystal structures of Gα – RGS complexes. Interacting residues are shown in orange. In the case of RGS2, which normally only regulates $G\alpha_q$, the interactions of the triple mutant – $G\alpha_{i3}$ complex are shown, as well as the interactions from the recently solved $G\alpha_q$ – RGS2 complex. The three residues highlighted in black color are the three mutations that enable RGS2 – $G\alpha_i$ interactions, without abolishing interactions with $G\alpha_q$. These residues interact with $G\alpha_q$ in wild type RGS2, and their mutations interact with $G\alpha_{i3}$. As it can be seen, different RGS domains use identical or conserved residues to contact different Gα subunits. Aligned sequences are the RGS domains of human RGS1

(UniProt: Q08116), RGS2 (UniProt: P41220), RGS3 (UniProt: P49796), RGS6 (UniProt: P49758), RGS7 (UniProt: P49802), RGS10 (UniProt: O43665), RGS12 (UniProt: O14924), RGS14 (UniProt: O43566), RGS18 (UniProt: Q9NS28), rat RGS4 (UniProt: P49799), bovine RGS9 (UniProt: O46469) and mouse (UniProt: P97428) RGS16. In the case of RGS14 there are structural data for interactions between $G\alpha_i$ and the GoLoco motif (PDB: 2XNS), however these are not presented here since the motif is not part of the RGS domain. Sequences were aligned with Clustal X 2.1 (Larkin et al., 2007) and the alignments were edited with JalView 2 (Clamp et al., 2004; Waterhouse et al., 2009).

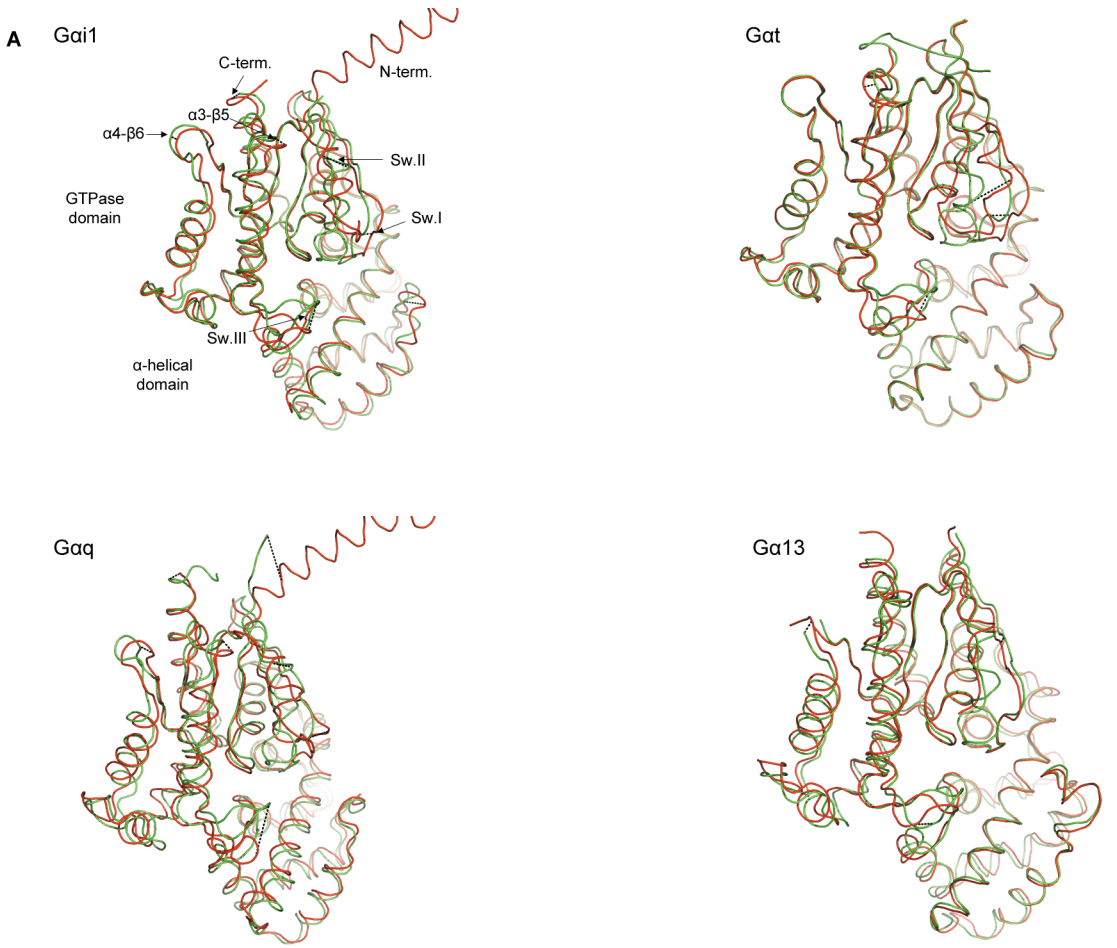

B

	Active:Inactive	N-term.	Sw. I	Sw. II	Sw. III	α3-β5	α4-β6	C-term.
$G\alpha_{i1}$	1GIA : 1GP2	–	T181: 3.5	H213: 5.4	E236: 4.9	W258: 2.4	D315: 1.5	K345: 2.3
$G\alpha_{t}$	1TND : 1TAG	–	T177: 2.9	K205: 7.5	V231: 3.4	A256: 2.4	R309: 0.4	–
$G\alpha_{q}$	3OHM : 3AH8	R35: 8.7	T187: 4.9	H218: 4.4	E241: 9.0	W263: 2.5	K322: 3.1	K354: 2.4
$G\alpha_{13}$	3CX8 : 1ZCB	–	E208: 1.3	–	R260: 4.0	N283: 1.6	D336: 2.1	–

Figure. S2. A. Comparison of active and inactive $G\alpha_{i1}$, $G\alpha_{t}$, $G\alpha_{q}$ and $G\alpha_{13}$ through structural alignment. Active subunits are green and inactive subunits are red. Important Gα structural elements are indicated in $G\alpha_{i1}$. All other subunits are shown in the same orientation, which is the same as in Figure. 1. The RMSD values of the alignments are presented in Table 3. **B.** A table of distances (in Å) between CA atoms of residues interacting with effectors, RGS proteins or GPCRs in active and inactive Gα subunits. Structures used are listed in the 'Active : Inactive' column (Chen et al., 2008; Coleman et al., 1994; Kreutz et al., 2006; Lambright et al., 1994;

Nishimura et al., 2010; Noel et al., 1993; Waldo et al., 2010; Wall et al., 1995). Residues are presented in the one letter code, followed by their position in each subunit sequence and the distance between active and inactive structures. The "–" sign is used for cases when there were no known interacting residues, or when parts of the structures were missing. All structural alignments were performed with Dali (Holm and Rosenstrom, 2010) and PyMol (DeLano, 2002).

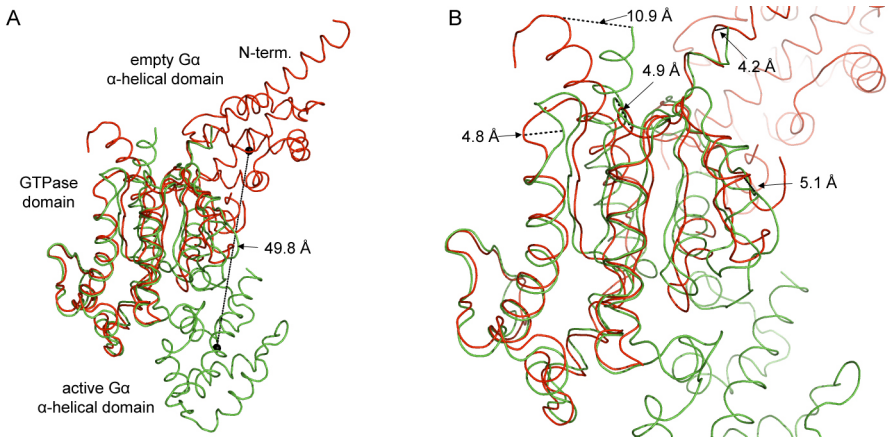

Figure. S3. Comparison of active and empty-state $G\alpha_s$ GTPase regions through structural alignment. Subunits are colored green and red for active and empty-state, respectively, and are shown in the same orientation as in Figure. S2. A) During nucleotide exchange, the α-helical domain moves vastly, resulting in the opening of the nucleotide cleft. The distance (in Å) is measured between the Centers of Gravity of the helical domains. B) View of the superimposed GTPase regions and measurement of distances. Structures used are active $G\alpha_s$ (PDB: 1AZT) (Sunahara et al., 1997) and intermediate $G\alpha_s$ (PDB: 3SN6) (Rasmussen et al., 2011).

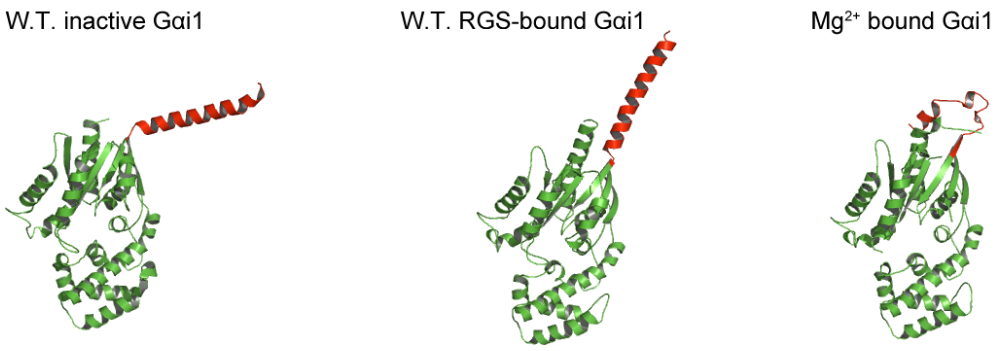

Figure. S4. The N-terminus (colored red) of Gα subunits may display significant flexibility. Comparison of inactive wild type Gβγ-bound $G\alpha_{i1}$ (PDB: 1GP2) (Wall et al., 1995) to Mg^{2+}GDP bound $G\alpha_{i1}$ mutant (PDB: 1BOF) in the presence of SO_4^- (Coleman and Sprang, 1998), and RGS4 bound $G\alpha_{i1}$ (PDB: 1AGR) (Tesmer et al., 1997a) shows vast movement of the N-terminus, which could account for its ability to participate in various interactions. This comparison shows that the presence of various interacting partners, such as Gβγ or RGS proteins (although in the case of RGS4 – bound $G\alpha_{i1}$ the conformation of the N-terminus may be attributed to crystal packing), as well as the presence of certain ions or mutations can result in many different N-terminal conformations. This flexibility may play an important part in the N-terminal helix's participation in various types of interactions.

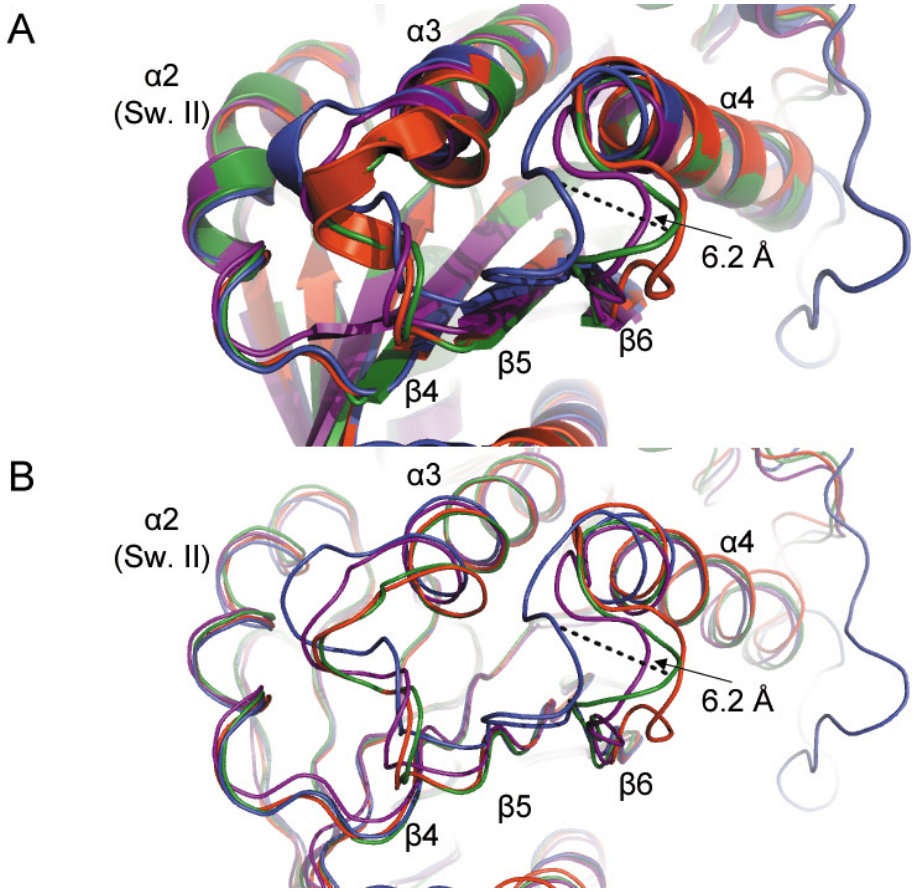

Figure. S5. Comparison of effector contact sites of $G\alpha_{i1}$, $G\alpha_s$, $G\alpha_q$ and $G\alpha_{12}$ in cartoon (**A**) and ribbon (**B**) representations, respectively. Switch II, α3 and α3-β5, which form the conserved effector binding site, as well as the α4-β6 loop, are compared. $G\alpha_{i1}$ (PDB: 1GIA) is green, $G\alpha_s$ (PDB: 1AZT) is blue, $G\alpha_q$ (PDB: 3AH8) is purple and $G\alpha_{12}$ (PDB: 1ZCA) (Kreutz et al., 2006) is red. The α2 (Switch II) and α3 helices show little or no differences, while the α3-β5 and α4-β6 loops differ in the four subunits. The $G\alpha_s$ α4-β6 loop is displaced ~5-6 Å from the position occupied by the α4-β6 loops of the other Gα subunits.

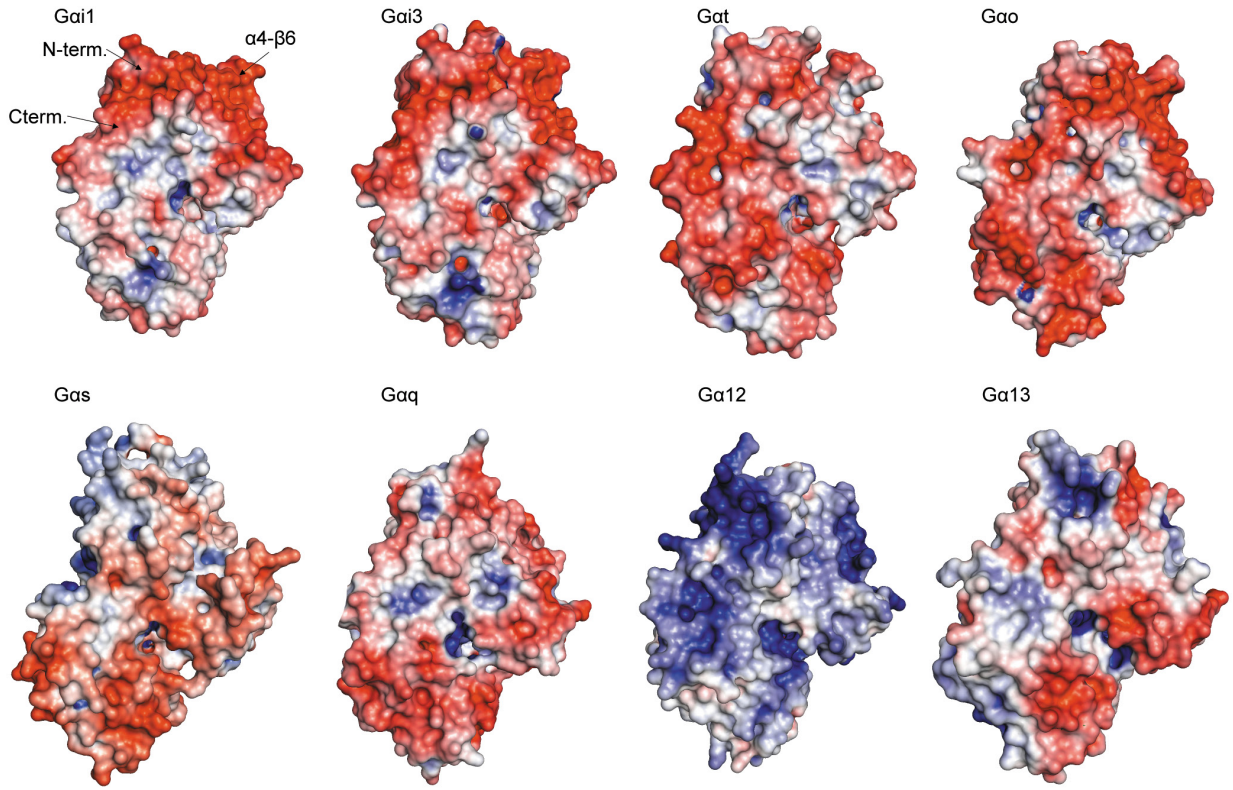

Figure. S6. Electrostatic molecular surfaces of Gα subunits. Subunit surfaces are contoured from -5 (red) to +5 (blue) kT/e^- based on the potential of the solvent accessible surface. The structures are rotated 180^o around a vertical axis, with respect to the representation shown in Figure. 2. Structures used are the same as in Figure 2. The N-terminal loop, C-terminus and the α4-β6 loop are identified on the $G\alpha_{i1}$ subunit. Calculations were performed with APBS(Baker et al., 2001) and PDB2PQR(Dolinsky et al., 2004; Dolinsky et al., 2007; Unni et al., 2011).

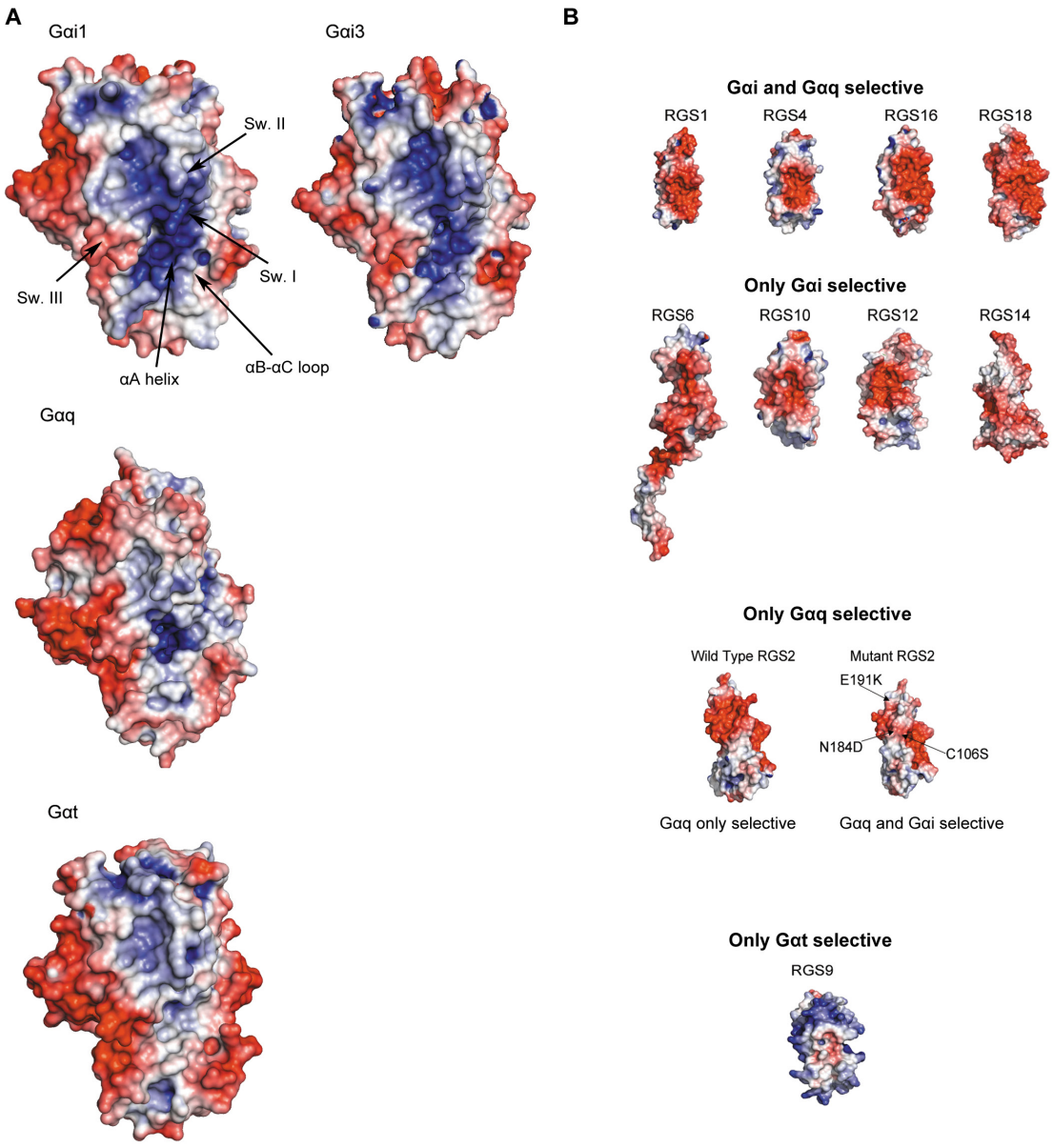

Figure S7. A. Electrostatic properties of known RGS interacting Gα subunits $G\alpha_{i1}$, $G\alpha_{i3}$, $G\alpha_{q}$ and $G\alpha_{t}$. All subunits are shown in the same orientation, which is the same as in Figure 1. Important structural features, including RGS interacting surfaces in the α-helical domain, are shown in $G\alpha_{i1}$. **B.** Electrostatic properties of various RGS domains. All structures are shown in the same orientation, which is their Gα interacting surface. RGS domains are grouped based on their interaction selectivity. $G\alpha_{i}$ and $G\alpha_{q}$ selective RGS proteins contact $G\alpha_{q}$ as well as $G\alpha_{i/o}$

families. $G\alpha_i$ selective RGS proteins contact all $G\alpha_{i1}$ and $G\alpha_{i3}$, but not $G\alpha_t$. RGS2, in its Wild Type form, contacts only $G\alpha_q$ and is the only member of the R4 subfamily of RGS proteins to show such selectivity. In its triple mutant form (C106S, N184D, E191K), it also regulates $G\alpha_i$ members. RGS9 contacts only $G\alpha_t$ but no other members of the $G\alpha_{i/o}$ family. The relatively positive electrostatic potential of its surface might be a factor in this selectivity. The $G\alpha_i$ only selective RGS domains show less negative surfaces compared to RGS proteins that contact both $G\alpha_{i/o}$ and $G\alpha_q$. Surfaces are contoured based on solvent accessible surface potential, from -5 kT/e^- (red) to +5 kT/e^- (blue). All Gα subunits come from the same structures used in Figures 2 and S6. RGS1, RGS4 and RGS16 come from crystal structures of complexes with $G\alpha_{i1}$ (PDB: 2GTP, PDB: 1AGR) (Soundararajan et al., 2008; Tesmer et al., 1997a) and $G\alpha_o$ (PDB: 3C7K) (Slep et al., 2008). RGS10 and RGS9 come from the structures of their complexes with $G\alpha_{i3}$ (PDB: 2IHB) (Soundararajan et al., 2008) and $G\alpha_t$ (PDB: 1FQK) (Slep et al., 2001), respectively. Wild type RGS2 comes from the structure of the unbound domain (PDB: 2AF0) (Soundararajan et al., 2008), while its mutant counterpart comes from the $G\alpha_{i3}$ – RGS2 complex (PDB: 2V4Z) (Kimple et al., 2009). RGS18 (PDB: 2JM5), RGS6 (PDB: 2ES0), RGS12 (PDB: 2EBZ) and RGS14 (PDB: 2JNU) are Solution NMR structures (Soundararajan et al., 2008).

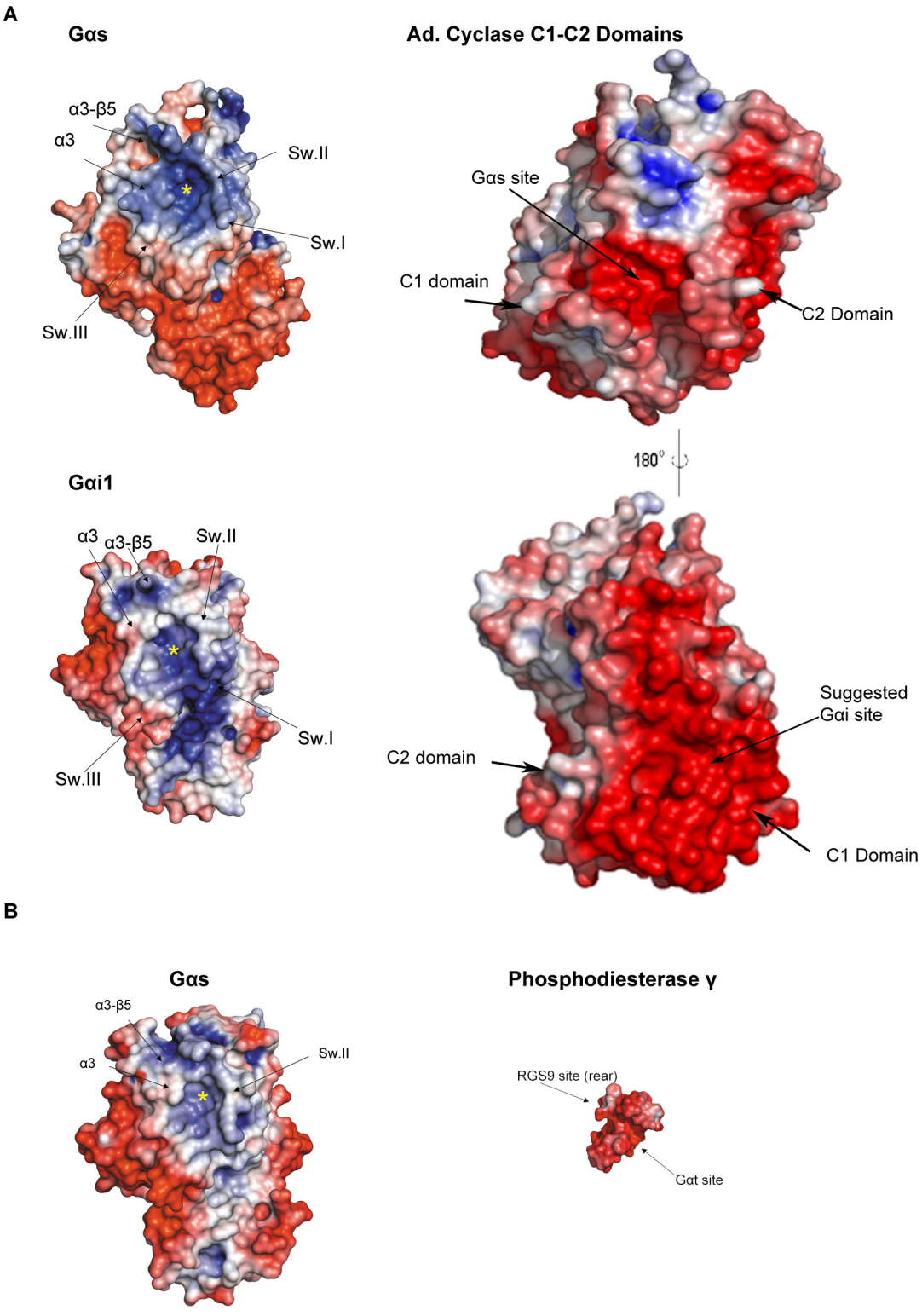

Figure S8. A. The electrostatic potential of Adenylyl Cyclase (A.C.) cytoplasmic C1 & C2 domains (right) and their interacting Gα subunits (left). The structure of A.C. (Tesmer et al.,

1997b) (PDB: 1AZS) contains the cytoplasmic domains C1 and C2, which form the active center of the enzyme. In the structures of $G\alpha_s$ (PDB: 1AZT) and $G\alpha_{i1}$ (PDB: 1GIA) important interaction sites are indicated with arrows, and the common effector binding pocket, formed by Switch II, α3, and the α3-β5 loop is indicated with a yellow asterisk. The $G\alpha_s$ interacting site of A.C. is formed mainly by the C2 domain, with a beta strand and a small loop from the C1 domain participating, and has been described by the $G\alpha_s$ – A.C. structure. The $G\alpha_i$ interacting site of A.C. has been suggested by biochemical studies, and is believed to include the C1 domain exclusively. **B.** The electrostatic potential of Phosphodiesterase γ (PDB: 1FQJ) (Slep et al., 2001) (right) and its relation to $G\alpha_t$ (left). In the structure of $G\alpha_t$ (PDB: 1TND) important interaction sites are indicated with arrows, and the common effector binding pocket, formed by Switch II, α3, and the α3-β5 loop is indicated with a yellow asterisk. Surfaces are contoured based on solvent accessible surface potential, from -5 kT/e^- (red) to +5 kT/e^- (blue).

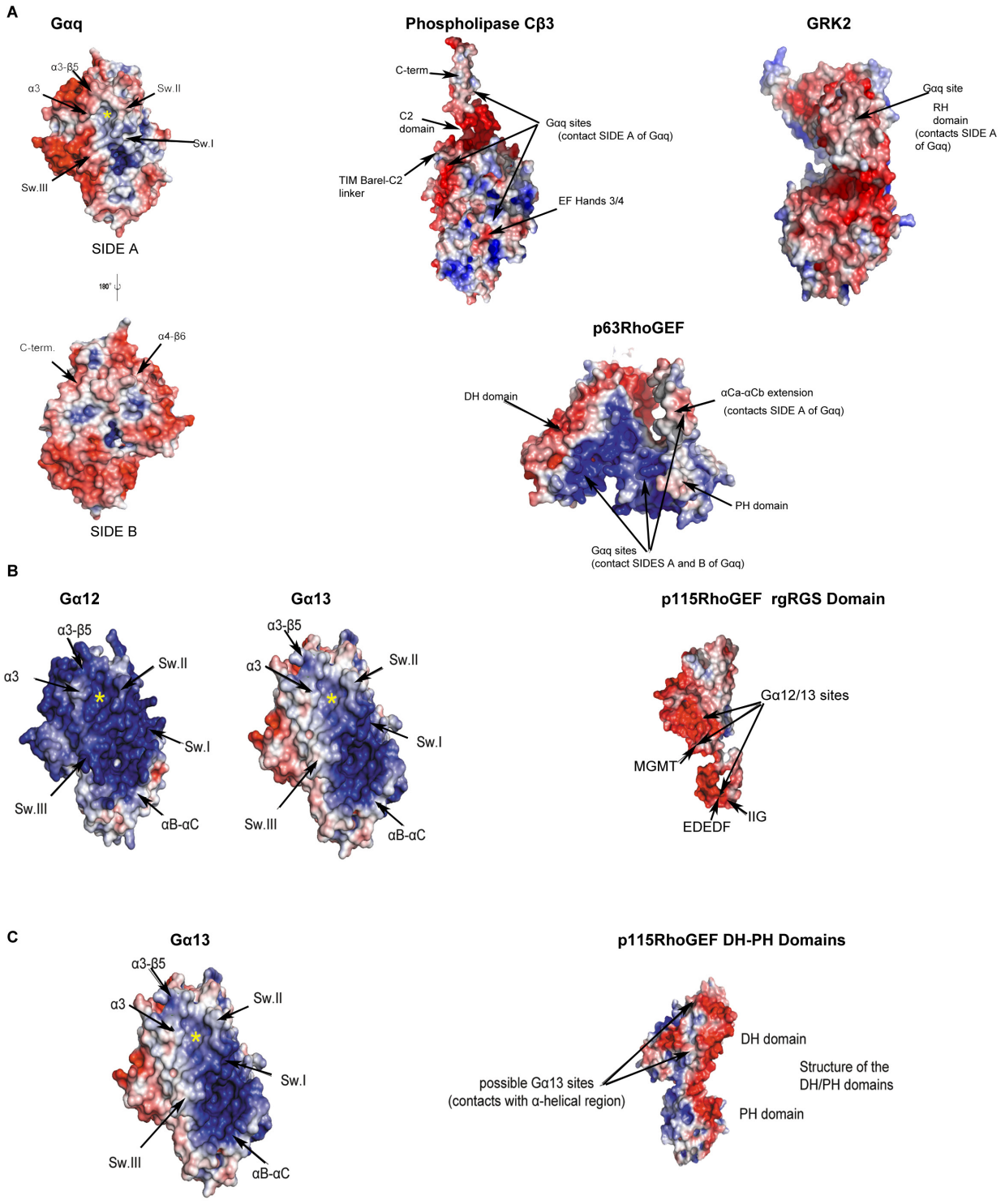

Figure S9. A. The electrostatic properties of $G\alpha_q$ – interacting effectors GRK2 (PDB: 2BCJ) (Tesmer et al., 2005), p63RhoGEF (PDB: 2RGN) (Chen et al., 2008) and Phospholipase $C\beta_3$

(PDB: 3OHM) (Waldo et al., 2010) (right) in relation to $G\alpha_q$ (left). In the structure of $G\alpha_q$ (PDB: 3OHM) important interaction sites are indicated with arrows, and the common effector binding pocket, formed by Switch II, α3, and the α3-β5 loop is indicated with a yellow asterisk. The side which contains the common effector site is labeled "SIDE A", and the opposite, containing the C-terminus and part of the α4-β6 loop, is labeled "SIDE B" for clarity. Important structural features of each effector, as well as Gα interacting surfaces are indicated with arrows. Effector surfaces that contact SIDE A or SIDE B of $G\alpha_q$ are labeled accordingly. **B.** The electrostatic potential of p115RhoGEF rgRGS domain (PDB: 1SHZ) (Chen et al., 2005) (right) and the members of the $G\alpha_{12/13}$ family (left). In the structures of $G\alpha_{12}$ (PDB: 1ZCA) and $G\alpha_{13}$ (PDB: 3CX8) important interaction sites are indicated with arrows, and the common effector binding pocket, formed by Switch II, α3, and the α3-β5 loop is indicated with a yellow asterisk. In the structure of p115RhoGEF important motifs are labeled. **C**. The electrostatic potential of $G\alpha_{13}$ and the structure of the DH/PH domains of p115RhoGEF (3ODO) (Chen et al., 2011). The structure for the complete p115RhoGEF has not been solved yet, however structures of the isolated rgRGS domain and the DH/PH domains are available, separated by a sequence of 185 residues of unknown structure. Proposed interacting surfaces are the αB-αC loop in the α-helical domain of $G\alpha_{13}$, and two surfaces in the DH domain of p115RhoGEF. Surfaces are contoured based on solvent accessible surface potential, from -5 kT/e^- (red) to +5 kT/e^- (blue).

Table S1. Crystal structures of Gα subunits deposited in the Protein DataBank (July 2012).

Index No.	Structure Name	PDB	PubMed	Gα type	Gα Chains	Resol. (Å)	R-value	Comments
1	G-protein Heterotrimer Gi α1 β1 γ2 with GDP bound	1GP2	8521505	Gαi1	A	2.30	0.226	→GDP bound →Gα – Gβγ complex
2	G-protein Heterotrimer Gi α1 (G203A) β1 γ2 with GDP bound	1GG2	8521505	Gαi1	A	2.30	0.205	→GDP bound →Mutation: G203A →Gα – Gβγ complex
3	Structure of Active Conformations of Giα1 and the mechanism of GTP hydrolysis	1GIA	8073283	Gαi1	A	2.00	0.175	→GTPγS bound →Truncated N-terminus
4	Structure of Active Conformations of Giα1 and the mechanism of GTP hydrolysis	1GFI	8073283	Gαi1	A	2.20	0.214	→GDP-AlF4- bound →Truncated N-terminus
5	Structure of Active Conformations of Giα1 and the mechanism of GTP hydrolysis	1GIL	8073283	Gαi1	A	2.30	0.222	→GTPγS bound →Truncated N-terminus →Mutation: Q204L
6	Structure of GTP-binding Protein	1GIT	8939752	Gαi1	A	2.60	0.186	→GDP-Pi bound →Truncated N-terminus →Mutation: G203A
7	GTPγS bound G42V Giα1	1AS0	9398294	Gαi1	A	2.00	0.206	→GTPγS bound →Truncated N-terminus →Mutation: G42V
8	GDP+Pi bound	1AS2	9398294	Gαi1	A	2.80	0.189	→GDP-Pi bound

	G42V Giα1							→Truncated N-terminus →Mutation: G42V
9	GDP bound G42V Giα1	1AS3	9398294	Gαi1	A	2.40	0.212	→GDP bound →Truncated N-terminus →Mutation: G42V
10	Complex of AlF4-activated Giα1 with RGS4	1AGR	9108480	Gαi1	A, D	2.80	0.216	→GDP-AlF4- bound →Gα – RGS complex
11	Giα1 bound to GDP and Magnesium	1BOF	9772163	Gαi1	A	2.20	0.227	→ GDP bound → Switch II, Switch III disordered
12	A326S mutant of an inhibitory α subunit	1BH2	9705312	Gαi1	A	2.10	0.190	→GTPγS bound →Truncated N-terminus →Mutation: A326S
13	Giα1 subunit of Guanine nucleotide-binding protein complexed with a GTP analogue	1CIP	10358003	Gαi1	A	1.50	0.213	→GppNHp bound →Truncated N-terminus
14	Crystal Structure of Human Gαi1 Bound to the GoLoco Motif of RGS14	1KJY	11976690	Gαi1	A, C	2.70	0.238	→GDP bound →Truncated N-terminus →Gα – RGS complex
15	Structure of the K180P mutant of Gi α subunit bound to AlF4 and GDP	1SVK	15128951	Gαi1	A	2.00	0.197	→GDP-AlF4- bound →Truncated N-terminus →Mutation: K180P
16	Structure of the K180P mutant of Gi α subunit bound to GppNHp	1SVS	15128951	Gαi1	A	1.50	0.200	→GppNHp bound →Truncated N-terminus →Mutation: K180P

17	Structure of Gαi1 bound to a GDP-selective peptide provides insight into guanine nucleotide exchange	1Y3A	16004878	Gαi1	A, B, C, D	2.50	0.255	→GDP bound →Truncated N-terminus →Gα – peptide complex → Switch III disordered
18	Structure of activated Gαi1 bound to a nucleotide-state-selective peptide: Minimal determinants for recognizing the active form of a G protein α subunit	2G83	16981699	Gαi1	A, B	2.80	0.301	→GDP-AlF4- bound →Truncated N-terminus →Gα – peptide complex
19	Crystal Structure Of Human Gαi1 Bound To The Goloco Motif Of Rgs14	2OM2	17603074	Gαi1	A, C	2.20	0.227	→GDP bound →Truncated N-terminus →Gα – RGS complex
20	Crystal structure of the heterodimeric complex of human RGS1 and activated Gi α 1	2GTP	18434541	Gαi1	A, B	2.55	0.228	→GDP-AlF4- bound →Truncated N-terminus →Gα – RGS complex
21	Crystal structure of the heterodimeric complex of human RGS16 and activated Gi α 1	2IK8	18434541	Gαi1	A, B	2.71	0.235	→GDP-AlF4- bound →Truncated N-terminus →Gα – RGS complex
22	Mechanism underlying the critical contribution of a switch II residue in a heterotrimeric G-protein α subunit during C. elegans asymmetric cell division	2EBC	18519563	Gαi1	A	2.24	0.229	→GDP bound → Switch II disordered → Mutation: G202D

23	Crystal Structure of a fast activating G protein mutant	3FFA	19703466	Gαi1	A	2.30	0.188	→GTPγS bound →Truncated N-terminus →Mutation: T329A
24	Giα1 mutant in GDP bound form	3FFB	19703466	Gαi1	A	2.57	0.181	→GDP bound →Truncated N-terminus →Switch II, Switch III disordered →Mutation: T329A
25	Crystal Structure of the G Protein Fast-Exchange Double Mutant I56C/Q333C	3D7M	19222191	Gαi1	A	2.90	0.249	→GDP-AlF4- bound →Truncated N-terminus →Mutation: I56C, Q333C
26	Structure of the K349P mutant of Gi α 1 subunit bound to ALF4 and GDP	2ZJY	-	Gαi1	A	2.80	0.181	→GDP-AlF4- bound →Truncated N-terminus →Mutation: K349P
27	Structure of the K349P mutant of Gi α 1 subunit bound to GDP	2ZJZ	-	Gαi1	A, B	2.60	0.221	→GDP bound →Truncated N-terminus →Mutation: K349P
28	Structure of a Gαi1 mutant with enhanced affinity for the RGS14 GoLoco motif.	3ONW	21115486	Gαi1	A, B	2.38	0.230	→GDP bound →Truncated N-terminus →Mutation: Q147L
29	Crystal structure of human Gαi1 bound to a designed helical peptide derived from the GoLoco motif of RGS14	2XNS	21388199	Gαi1	A, B	3.41	0.223	→GDP bound →Truncated N-terminus
30	Crystal structure of the G202A mutant of human	3UMS	20351284	Gαi1	A	2.34	0.183	→GDP bound →Truncated N-terminus

	Gαi1							→Switch II disordered →Mutation: G202A
31	A Gαi1 P-loop mutation prevents transition to the activated state	3QE0	22383884	Gαi1	A, B C	3.00	0.249	→GDP bound →Truncated N-terminus →Switch II disordered →Mutation: G42R
32	A Gα P-loop mutation prevents transition to the activated state: G42R bound to RGS14 GoLoco	3QI2	22383884	Gαi1	A, B	2.80	0.200	→GDP bound →Truncated N-terminus →Mutation: G42R →Gα – RGS complex
33	Structure of LGN GL4/Gα1 complex	4G5Q	-	Gαi1	A, B, C, D	2.90	0.209	→GDP bound →Truncated N-terminus →Gα – G-protein signaling modulator complex
34	Crystal structure of the heterodimeric complex of human RGS8 and activated Giα3	2ODE	18434541	Gαi3	A, C	1.90	0.181	→GDP-AlF4- bound →Truncated N-terminus →Gα – RGS complex
35	Crystal structure of the heterodimeric complex of human RGS10 and activated Giα3	2IHB	18434541	Gαi3	A	2.71	0.209	→GDP-AlF4- bound →Truncated N-terminus →Gα – RGS complex
36	The crystal structure of the human G-protein subunit α (GNAI3) in complex with an engineered Regulator of G-Protein Signaling Type 2 domain	2V4Z	19478087	Gαi3	A	2.80	0.210	→GDP-AlF4- bound →Truncated N-terminus →Gα – RGS complex

	(RGS2)							
37	Structure of LGN GL4/Gαi3(Q147L) complex	4G5O	-	Gαi3	A, B, C, D	2.90	0.210	→GDP bound →Truncated N-terminus →Mutation: Q147L →Gα – G-protein signaling modulator complex
38	Structure of LGN GL4/Gαi3 complex	4G5R	-	Gαi3	A, B, C, D	3.48	0.211	→GDP bound →Truncated N-terminus →Gα – G-protein signaling modulator complex
39	Structure of LGN GL4/Gαi3 complex	4G5S	-	Gαi3	A, B, C, D	3.62	0.210	→GDP bound →Truncated N-terminus →Gα – G-protein signaling modulator complex
40	The 2.2 Angstroms crystal structure of Transducin-α complexed with GTPγS	1TND	8259210	Gαt	A, B, C	2.20	0.190	→GTPγS bound →Truncated N-terminus
41	Structural determinants for activation of the α-subunit of a heterotrimeric G protein.	1TAG	8208289	Gαt	A	1.80	0.187	→GDP bound →Truncated N-terminus
42	GTPase mechanism of Gproteins from the 1.7-A crystal structure of transducin α-GDP-AIF-4	1TAD	7969474	Gαt	A, B, C	1.70	0.209	→GDP-AlF4- bound →Truncated N-terminus
43	Heterotrimeric complex of a Gtα/Giα chimera and the Gtβγ	1GOT	8552184	Gαt	A	2.00	0.207	→GDP bound →Chimera: 216-294 of Gαt have been replaced

	subunits							with 220-298 of Gαi1 →Gα – Gβγ complex
44	Crystal structure of the heterotrimeric complex of the RGS domain of RGS9, the γ subunit of Phosphodiesterase and the Gt/i1 chimera α subunit [(RGS9)-(PDEγ)-(Gt/i1α)-(GDP)-(AlF4-)-(Mg2+)]	1FQJ	11234020	Gαt	A, D	2.02	0.233	→GDP-AlF4- bound →Truncated N-terminus →Chimera: 216-294 of Gαt have been replaced with 220-298 of Gαi1 →Gα – effector – RGS complex
45	Crystal structure of the heterodimeric complex of the RGS domain of RGS9, and the Gt/i1 chimera α subunit [(RGS9)-(Gt/i1α)-(GDP)-(AlF4-)-(Mg2+)]	1FQK	11234020	Gαt	A, C	2.30	0.231	→GDP-AlF4- bound →Truncated N-terminus →Chimera: 216-294 of Gαt have been replaced with 220-298 of Gαi1 →Gα – RGS complex
46	Studies of a constitutively active G-alpha subunit provide insights into the mechanism of G protein activation.	3V00	22448927	Gαt	A, B, C	2.90	0.221	→Chimera: 216-294 of Gαt have been replaced with 220-298 of Gαi1 →Mutation: G56P, K244H, D247N
47	Molecular architecture of Galphao and the structural basis for RGS16-mediated deactivation	3C7K	18434540	Gαo	A, C	2.90	0.250	→GDP-AlF4- bound →Truncated N-terminus →Gα – RGS complex
48	Gsα complexed with GTPγS	1AZT	9395396	Gαs	A, B	2.30	0.219	→GTPγS bound →Truncated N-terminus → A part of α-helical domain disordered

49	Complex of Gsα with the Catalytic domains of mammalian Adenylyl cyclase	1AZS	9417641	Gαs	C	2.30	0.219	→GTPγS bound →Truncated N-terminus → A part of α-helical domain disordered →Gα – effector complex
50	Complex of Gsα with the Catalytic domains of mammalian Adenylyl cyclase: Complex with Adenosine 5'-(α thio) triphosphate (RP), Mg and Mn	1CJK	10427002	Gαs	C	3.00	0.220	→GTPγS bound →Truncated N-terminus → A part of α-helical domain disordered →Gα – effector complex
51	Complex of Gsα with the Catalytic domains of mammalian Adenylyl cyclase: Complex with β-L-2'-3'-dideoxyATP, Mn and Mg	1CJT	10427002	Gαs	C	2.80	0.206	→GTPγS bound →Truncated N-terminus → A part of α-helical domain disordered →Gα – effector complex
52	Complex of Gsα with the Catalytic domains of mammalian Adenylyl cyclase: Complex with β-L-2'-3'-dideoxyATP and Mg	1CJU	10427002	Gαs	C	2.80	0.222	→GTPγS bound →Truncated N-terminus → A part of α-helical domain disordered →Gα – effector complex
53	Complex of Gsα with the Catalytic domains of mammalian Adenylyl cyclase: Complex with β-L-2'-3'-dideoxyATP, Mg and Zn	1CJV	10427002	Gαs	C	3.00	0.203	→GTPγS bound →Truncated N-terminus → A part of α-helical domain disordered →Gα – effector complex
54	Complex of Gsα with the Catalytic domains of mammalian Adenylyl cyclase:	1CS4	11087399	Gαs	C	2.50	0.221	→GTPγS bound →Truncated N-terminus → A part of α-helical

	Complex with 2'-deoxy-Adenosine 3'-monophosphate, pyrophosphate and Mg							domain disordered →Gα – effector complex
55	Complex of Gsα with the Catalytic domains of mammalian Adenylyl cyclase: Complex with 2'-deoxy-Adenosine 3'-triphosphate and Mg	1CUL	11087399	Gαs	C	2.40	0.221	→GTPγS bound →Truncated N-terminus → A part of α-helical domain disordered →Gα – effector complex
56	Complex Of Gs- With The Catalytic Domains Of Mammalian Adenylyl Cyclase: Complex With 2'(3')-O-(N-methylanthraniloyl)-guanosine 5'-triphosphate and Mn	1TL7	15591060	Gαs	C	2.80	0.254	→GTPγS bound →Truncated N-terminus → A part of α-helical domain disordered →Gα – effector complex
57	Structural basis for the inhibition of mammalian Adenylyl Cyclase by MANT-GTP	1U0H	15591060	Gαs	C	2.90	0.245	→GTPγS bound →Truncated N-terminus → A part of α-helical domain disordered →Gα – effector complex
58	Complex Of Gs- With The Catalytic Domains Of Mammalian Adenylyl Cyclase: Complex With TNP-ATP and Mn	2GVD	16766715	Gαs	C	2.90	0.245	→GTPγS bound →Truncated N-terminus → A part of α-helical domain disordered →Gα – effector complex
59	Crystal Structure of Complex of Gs- with The Catalytic Domains of Mammalian	2GVZ	16766715	Gαs	C	3.27	0.275	→GTPγS bound →Truncated N-terminus → A part of α-helical domain disordered

	Adenylyl Cyclase: Complex with MANT-ATP and Mn							→Gα – effector complex
60	Complex of GS-α with the Catalytic Domains of Mammalian Adenylyl Cyclase: Complex with Pyrophosphate and Ca	3C14	19243146	Gαs	C	2.68	0.248	→GTPγS bound →Truncated N-terminus → A part of α-helical domain disordered →Gα – effector complex
61	Complex of GS-α with the Catalytic Domains of Mammalian Adenylyl Cyclase: Complex with Pyrophosphate and Mg	3C15	19243146	Gαs	C	2.78	0.240	→GTPγS bound →Truncated N-terminus → A part of α-helical domain disordered →Gα – effector complex
62	Complex of GS-α with the Catalytic Domains of Mammalian Adenylyl Cyclase: Complex with Adenosine-5'-Triphosphate and Ca	3C16	19243146	Gαs	C	2.87	0.252	→GTPγS bound →Truncated N-terminus → A part of α-helical domain disordered →Gα – effector complex
63	Complex of GS-α with the Catalytic Domains of Mammalian Adenylyl Cyclase: Complex with Adenosine 5-O-(l-Thiophosphate) and Low Ca Concentration	3MAA	19243146	Gαs	C	3.00	0.242	→GTPγS bound →Truncated N-terminus → A part of α-helical domain disordered →Gα – effector complex
64	Complex of GS-α with the catalytic domains of mammalian adenylyl cyclase: complex with MANT-ITP and Mn	3G82	-	Gαs	C	3.11	0.240	→GTPγS bound →Truncated N-terminus → A part of α-helical domain disordered →Gα – effector complex

65	Crystal structure of the β2 adrenergic receptor-Gs protein complex	3SN6	21772288	Gαs	A	3.20	0.228	→No nucleotide bound → Helical domain moves to open nucleotide cleft →Mutation: G72S →Gα – Gβγ – receptor complex
66	Crystal Structure of G Protein-Coupled Receptor Kinase 2 in Complex with Gα-q and Gβγ Subunits	2BCJ	16339447	Gαq	Q	3.06	0.236	→GDP-AlF4- bound →Truncated N-terminus →Chimera: N-terminus from Gαi1 →Gα – effector complex
67	Crystal Structure of p63RhoGEF complex with Gα-q and RhoA	2RGN	18096806	Gαq	A, D	3.50	0.243	→GDP-AlF4- bound →Truncated N-terminus →Chimera: N-terminus from Gαi1 →Gα – effector complex
68	Structure of heterotrimeric G protein Gα-q beta gamma in complex with an inhibitor YM-254890	3AH8	20639466	Gαq	A	2.90	0.262	→GDP bound →Chimera: N-terminus from Gαi1 →Gα – Gβγ – inhibitor peptide complex
69	Structure of human regulator of G protein signaling 2 (RGS2) in complex with murine Galpha-q(R183C)	4EKD	-	Gαq	A	2.71	0.193	→GDP-AlF4- bound →Truncated N-terminus →Gα – RGS complex →Mutations: E125D, N126V, Y128D, V129Y, D130A, R183C
70	Structure of human regulator of G protein signaling 2 (RGS2) in complex with murine Galpha-q(R183C)	4EKC	-	Gαq	A	7.40	0.161	→GDP-AlF4- bound →Truncated N-terminus →Gα – RGS complex →Mutations: E125D, N126V, Y128D, V129Y,

								D130A, R183C
71	Crystal structure of activated G α Q bound to its effector phospholipase C β 3	3OHM	20966218	Gαq	A	2.70	0.207	→GDP-AlF4- bound →Truncated N-terminus →Gα – effector complex
72	Crystal structure of G α 12 in complex with GDP, Mg2+ and AlF4-	1ZCA	16388592	Gα12	A, B	2.90	0.239	→GDP-AlF4- bound →Truncated N-terminus →Chimera: N-terminus from Gαi1
73	Crystal structure of G α 13 in complex with GDP	1ZCB	16388592	Gα13	A	2.00	0.209	→GDP bound →Truncated N-terminus →Chimera: N-terminus from Gαi1 →Switch II, α4-β6 disordered
74	Crystal Structure of the p115RhoGEF rgRGS Domain in A Complex with Gα(13):Gα(i1) Chimera	1SHZ	15665872	Gα13	A, D	2.85	0.229	→GDP-AlF4- bound →Truncated N-terminus →Chimera: residues 21-47, 185-210, 213-230, 240-353 of Gαi1 and residues 64-207, 234-235, 254-262 of Gα13 →Gα – effector complex
75	Crystal Structure of PDZRhoGEF rgRGS Domain in a Complex with Galpha-13 Bound to GDP	3CX6	18940608	Gα13	A	2.50	0.266	→GDP bound →forced active conformation →Truncated N-terminus →α4-β6 disordered →Gα – effector complex
76	Crystal Structure of PDZRhoGEF rgRGS Domain in a Complex with	3CX7	18940608	Gα13	A	2.25	0.264	→GDP-AlF4 bound →Truncated N-terminus

	Galpha-13 Bound to GDP-AlF4							→α4-β6 disordered →Gα – effector complex
77	Crystal Structure of PDZRhoGEF rgRGS Domain in a Complex with Galpha-13 Bound to GTPγS	3CX8	18940608	Gα13	A	2.00	0.243	→GTPγS bound →Truncated N-terminus →α4-β6 disordered →Gα – effector complex
78	Crystal structure of p115RhoGEF RGS domain in complex with G α 13	3AB3	21507947	Gα13	A, C	2.40	0.205	→GDP-AlF4 bound →Truncated N-terminus →Chimera: N-terminus from Gαi3 →α4-β6 disordered →Gα – effector complex
79	Crystal structure of the Gα protein ATGPA 1 from Arabidopsis thaliana	2XTZ	21304159	GPA1	A, B, C	2.34	0.212	→GTPγS bound →Truncated N-terminus →Plant G-protein

Table S2. RMSD values (Å) of aligned active conformations of different Gα families and subfamilies.

	$G\alpha_{i3}$ (2V4Z.A)	*Gαt (1TND.A)*	*$G\alpha_{o}$ (3C7K.A)*	*$G\alpha_{s}$ (1AZT.A)*	*$G\alpha_{q}$ (3OHM.A)*	*$G\alpha_{12}$ (1ZCA.A)*	*$G\alpha_{13}$ (3CX8.A)*
$G\alpha_{i1}$ (1GIA.A)	0.9	1.0	1.0	1.8	1.4	1.5	1.3
$G\alpha_{i3}$ (2V4Z.A)		0.9	1.0	1.7	1.4	1.6	1.3
$G\alpha_{t}$ (1TND.A)			0.9	1.5	1.5	1.7	1.4
$G\alpha_{o}$ (3C7K.A)				1.5	1.3	1.5	1.5
$G\alpha_{s}$ (1AZT.A)					1.7	1.7	1.4
$G\alpha_{q}$ (3OHM.A)						1.5	1.2
$G\alpha_{12}$ (1ZCA.A)							1.1

Table S3. RMSD values (Å) of aligned inactive conformations (where available) of different Gα families and subfamilies.

	$G\alpha_t$ *(1TAG.A)*	$G\alpha_q$ *(3AH8.A)*	$G\alpha_{13}$ *(1ZCB.A)*
$G\alpha_{i1}$ *(1GP2.A)*	1.5	2.1	1.7
$G\alpha_t$ *(1TAG.A)*		2.4	2.0
$G\alpha_q$ *(3AH8.A)*			2.6

Table S4. Energy calculations of Gα – RGS complexes, according to HADDOCK (de Vries et al., 2010).

Complex	Index No.[a]	PDB	Interface	Ions	E_{VDW}[b] (kcal/mol)	E_{ELE}[b] (kcal/mol)	E_{DES}[b] (kcal/mol)	BSA[b] (Å^2)
$G\alpha_{i1}$– RGS4	10	1AGR	A (Gαi1) - E (RGS4)	Mg^{2+}	-43.4 ±2.4	-536.9 ±11.1	45.7 ±3.0	1819.6
$G\alpha_{i1}$– RGS1	20	2GTP	A ($G\alpha_{i1}$) - C (RGS1)	Mg^{2+}	-58.4 ±1.3	-450.7 ±11.8	39.7 ±2.9	1819.7
$G\alpha_{i1}$– RGS16	21	2IK8	A ($G\alpha_{i1}$) - B (RGS16)	Mg^{2+}	-45.9 ±1.7	-556.0 ±37.9	48.5 ±8.6	1770.0
$G\alpha_{i3}$– RGS10	35	2IHB	A ($G\alpha_{i3}$) - B (RGS10)	Mg^{2+}	-46.9 ±1.8	-524.0 ±19.7	56.9 ±4.0	1774.0
$G\alpha_{i3}$– RGS8	34	2ODE	A ($G\alpha_{i3}$) - B (RGS8)	Mg^{2+}	-47,8 ±4.2	-472.3 ±10.6	56.9 ±5.9	1886.6
$G\alpha_{i3}$– RGS2 mutant	36	2V4Z	A ($G\alpha_{i3}$) - B (RGS2 mutant)	Mg^{2+}	-57.1 ±2.2	-332.3 ±21.6	41.1 ±2.6	1743.2
$G\alpha_{t}$– RGS9	45	1FQK	A ($G\alpha_{t}$) - B (RGS9)	Mg^{2+}	-48.2 ±2.4	-576.4 ±47.3	58.8 ±11.8	1886.2
$G\alpha_{o}$– RGS16	47	3C7K	A ($G\alpha_{o}$) - B (RGS16)	Mg^{2+}	-55.9 ±4.7	-593.5 ±30.1	61.6 ±2.6	2016.4
$G\alpha_{q}$– RGS2 wild type	69	4EKD	A ($G\alpha_{q}$) - B (RGS2 wild)	Mg^{2+}	-58.7 ±2.1	-561.7 ±28.7	40.4 ±9.4	2241.5

a: Index number in Table S1. Readers can refer to Table S1 for properties of each structure.

b: E_{VDW}=van der Waals energy, E_{ELE}=electrostatic energy, E_{DES}=desolvation energy, BSA=buried surface area.

Table S5. Energy calculations of Gα – effector complexes, according to HADDOCK (de Vries et al., 2010).

Complex	Index No.	PDB	Interface	Ions	E_{VDW} (kcal/mol)	E_{ELE} (kcal/mol)	E_{DES} (kcal/mol)	BSA ($Å^2$)
$G\alpha_s$ – Ad. Cyclase C1/C2 domains	49	1AZS	A (C1 domain AC) - C ($G\alpha_s$)	Mg^{2+}	-24.2 ±0.5	-34.6 ±6.6	7.3 ±3.3	609.0
			B (C2 domain AC) - C ($G\alpha_s$)	Mg^{2+}	-56.3 ±2.5	-263.8 ±15.1	0.3 ±2.2	1589.6
$G\alpha_{t/i}$ – PDEγ – RGS9	44	1FQJ	A ($G\alpha_{t/i}$) – B (RGS9)	Mg^{2+}	-48.5 ±0.9	-634.6 ±16.7	34.0 ±5.7	2013.8
			A ($G\alpha_t$) – B (PDEγ)	Mg^{2+}	-63.7 ±2.6	-257.2 ±8.0	-10.4 ±2.5	1591.9
$G\alpha_q$ – $PLC\beta_3$	71	3OHM	A ($G\alpha_q$) – B ($PLC\beta_3$)	Mg^{2+} Ca^{2+}	-101.9 ±3.8	-531.2 ±16.9	30.2 ±5.1	2995.1
$G\alpha_q$ – GRK2 - Gβγ	66	2BCJ	A (GRK2) – Q ($G\alpha_q$)	Mg^{2+}	-60.9 ±1.4	-187.9 ±10.0	85.3 ±6.2	1624.1
$G\alpha_q$ – p63RhoGEF - RhoA	67	2RGN	A ($G\alpha_q$) – B (p63RhoGEF)	Mg^{2+}	-113.1 ±5.4	625.3 ±39.5	56.8 ±6.1	3579.7
$G\alpha_{13/i}$ – p115RhoGEF	74	1SHZ	A ($G\alpha_{13/i}$) – C (p115-rgRGS)	Mg^{2+}	-79.4 ±1.0	-875.1 ±38.1	14.8 ±6.2	3155.1
$G\alpha_{13}$ – p115RhoGEF	78	3AB3	A ($G\alpha_{13}$) – B (p115-rgRGS)	Mg^{2+}	-98.1 ±3.4	-811.1 ±8.3	56.5 ±3.6	3338.1
$G\alpha_{13}$ – PDZRhoGEF	77	3CX8	A ($G\alpha_{13}$) – B (PDZ-rgRGS)	Mg^{2+}	-95.3 ±5.2	-657.6 ±46.5	44.7 ±4.4	3078.7

REFERENCES

Baker, N.A., D. Sept, S. Joseph, M.J. Holst, J.A. McCammon, 2001. Electrostatics of nanosystems: application to microtubules and the ribosome. Proc Natl Acad Sci U S A 98, 10037-10041.

Chen, Z., W.D. Singer, P.C. Sternweis, S.R. Sprang, 2005. Structure of the p115RhoGEF rgRGS domain-Galpha13/i1 chimera complex suggests convergent evolution of a GTPase activator. Nat Struct Mol Biol 12, 191-197.

Chen, Z., L. Guo, S.R. Sprang, P.C. Sternweis, 2011. Modulation of a GEF switch: autoinhibition of the intrinsic guanine nucleotide exchange activity of p115-RhoGEF. Protein Sci 20, 107-117.

Chen, Z., W.D. Singer, S.M. Danesh, P.C. Sternweis, S.R. Sprang, 2008. Recognition of the activated states of Galpha13 by the rgRGS domain of PDZRhoGEF. Structure 16, 1532-1543.

Clamp, M., J. Cuff, S.M. Searle, G.J. Barton, 2004. The Jalview Java alignment editor. Bioinformatics 20, 426-427.

Coleman, D.E., S.R. Sprang, 1998. Crystal structures of the G protein Gi alpha 1 complexed with GDP and Mg2+: a crystallographic titration experiment. Biochemistry 37, 14376-14385.

Coleman, D.E., A.M. Berghuis, E. Lee, M.E. Linder, A.G. Gilman*, et al.*, 1994. Structures of active conformations of Gi alpha 1 and the mechanism of GTP hydrolysis. Science 265, 1405-1412.

de Vries, S.J., M. van Dijk, A.M. Bonvin, 2010. The HADDOCK web server for data-driven biomolecular docking. Nat. Protoc. 5, 883-897.

DeLano, W.L., 2002. The Pymol Molecular Graphics System. DeLano Scientific, San Carlos, CA, USA.

Dolinsky, T.J., J.E. Nielsen, J.A. McCammon, N.A. Baker, 2004. PDB2PQR: an automated pipeline for the setup of Poisson-Boltzmann electrostatics calculations. Nucleic. Acids. Res. 32, W665-667.

Dolinsky, T.J., P. Czodrowski, H. Li, J.E. Nielsen, J.H. Jensen*, et al.*, 2007. PDB2PQR: expanding and upgrading automated preparation of biomolecular structures for molecular simulations. Nucleic. Acids. Res. 35, W522-525.

Holm, L., P. Rosenstrom, 2010. Dali server: conservation mapping in 3D. Nucleic. Acids. Res. 38, W545-549.

Kimple, A.J., M. Soundararajan, S.Q. Hutsell, A.K. Roos, D.J. Urban*, et al.*, 2009. Structural determinants of G-protein alpha subunit selectivity by regulator of G-protein signaling 2 (RGS2). J. Biol. Chem. 284, 19402-19411.

Kreutz, B., D.M. Yau, M.R. Nance, S. Tanabe, J.J. Tesmer*, et al.*, 2006. A new approach to producing functional G alpha subunits yields the activated and deactivated structures of G alpha(12/13) proteins. Biochemistry 45, 167-174.

Lambright, D.G., J.P. Noel, H.E. Hamm, P.B. Sigler, 1994. Structural determinants for activation of the alpha-subunit of a heterotrimeric G protein. Nature 369, 621-628.

Larkin, M.A., G. Blackshields, N.P. Brown, R. Chenna, P.A. McGettigan*, et al.*, 2007. Clustal W and Clustal X version 2.0. Bioinformatics 23, 2947-2948.

Nishimura, A., K. Kitano, J. Takasaki, M. Taniguchi, N. Mizuno*, et al.*, 2010. Structural basis for the specific inhibition of heterotrimeric Gq protein by a small molecule. Proc Natl Acad Sci U S A 107, 13666-13671.

Noel, J.P., H.E. Hamm, P.B. Sigler, 1993. The 2.2 A crystal structure of transducin-alpha complexed with GTP gamma S. Nature 366, 654-663.

Rasmussen, S.G., B.T. DeVree, Y. Zou, A.C. Kruse, K.Y. Chung*, et al.*, 2011. Crystal structure of the beta2 adrenergic receptor-Gs protein complex. Nature 477, 549-555.

Slep, K.C., M.A. Kercher, W. He, C.W. Cowan, T.G. Wensel*, et al.*, 2001. Structural determinants for regulation of phosphodiesterase by a G protein at 2.0 A. Nature 409, 1071-1077.

Slep, K.C., M.A. Kercher, T. Wieland, C.K. Chen, M.I. Simon*, et al.*, 2008. Molecular architecture of Galphao and the structural basis for RGS16-mediated deactivation. Proc Natl Acad Sci U S A 105, 6243-6248.

Soundararajan, M., F.S. Willard, A.J. Kimple, A.P. Turnbull, L.J. Ball*, et al.*, 2008. Structural diversity in the RGS domain and its interaction with heterotrimeric G protein alpha-subunits. Proc Natl Acad Sci U S A 105, 6457-6462.

Sunahara, R.K., J.J. Tesmer, A.G. Gilman, S.R. Sprang, 1997. Crystal structure of the adenylyl cyclase activator Gsalpha. Science 278, 1943-1947.

Tesmer, J.J., D.M. Berman, A.G. Gilman, S.R. Sprang, 1997a. Structure of RGS4 bound to AlF4--activated G(i alpha1): stabilization of the transition state for GTP hydrolysis. Cell 89, 251-261.

Tesmer, J.J., R.K. Sunahara, A.G. Gilman, S.R. Sprang, 1997b. Crystal structure of the catalytic domains of adenylyl cyclase in a complex with Gsalpha.GTPgammaS. Science 278, 1907-1916.

Tesmer, V.M., T. Kawano, A. Shankaranarayanan, T. Kozasa, J.J. Tesmer, 2005. Snapshot of activated G proteins at the membrane: the Galphaq-GRK2-Gbetagamma complex. Science 310, 1686-1690.

Unni, S., Y. Huang, R.M. Hanson, M. Tobias, S. Krishnan*, et al.*, 2011. Web servers and services for electrostatics calculations with APBS and PDB2PQR. J. Comput. Chem. 32, 1488-1491.

Waldo, G.L., T.K. Ricks, S.N. Hicks, M.L. Cheever, T. Kawano*, et al.*, 2010. Kinetic scaffolding mediated by a phospholipase C-beta and Gq signaling complex. Science 330, 974-980.

Wall, M.A., D.E. Coleman, E. Lee, J.A. Iniguez-Lluhi, B.A. Posner*, et al.*, 1995. The structure of the G protein heterotrimer Gi alpha 1 beta 1 gamma 2. Cell 83, 1047-1058.

Waterhouse, A.M., J.B. Procter, D.M. Martin, M. Clamp, G.J. Barton, 2009. Jalview Version 2--a multiple sequence alignment editor and analysis workbench. Bioinformatics 25, 1189-1191.